Physica Scripta. Vol. 67, 414–419, 2003

Identification of n = 4, Δn = 0 Transitions in the Spectra of Nickel-like Cadmium Ions from a Capillary Discharge Plasma Column

A. Rahman[1], E. C. Hammarsten[1], S. Sakadzic[1], J. J. Rocca[1,*] and J.-F. Wyart[2,**]

[1] Electrical and Computer Engineering Department, Colorado State University, Fort Collins, CO 80523, USA
[2] Laboratoire Aime Cotton, CNRS (UPR 3321), Centre Universitaire, 91405-Orsay, France

Received December 11, 2002; accepted December 27, 2002

PACS Ref: 32.30, 32.70, 42.55.

Abstract

Spectra of Nickel-like Cadmium (CdXXI) ions in the 12.7–18.4 nm wavelength region obtained with a high current capillary discharge have been analyzed. Fifty-three $3d^9\,4p$–$3d^9\,4d$ and $3d^9\,4d$–$3d^9\,4f$ CdXXI lines were identified with the assistance of calculations performed using the Slater–Condon method with generalized least-squares fits of the energy parameters. The average deviation between the measured and theoretical wavelengths is $\langle \lambda\,\text{exp}-\lambda\text{th} \rangle = 0.0065$ nm. The results demonstrate that fast capillary discharges can produce high quality spectra for the study of multiply charged ions with charges of up to at least $Z = 20$.

1. Introduction

There is significant interest in the spectra of Ni-like ions in relation to the development of soft X-ray lasers [1–4]. Of particular interest is the spectrum of Ni-like cadmium in relation to the development of efficient lasers for metrology applications in the vicinity of 13.5 nm, the wavelength that has been selected for the nanolithography to be used in the future generations of integrated circuits. Laser amplification can be obtained at 13.2 nm by creating a population inversion between the $3d^9\,4d\,^1S_0$–$3d^9\,4p\,^1P_1$ levels of Ni-like CdXXI [2].

Several previous works have studied the energy level structure and oscillator strengths of Ni-like Cd ions. Transitions to the ground state $3d^{10}$ were observed at low resolution in [5] and surveyed theoretically by MCDF [6], parametric potential [7] and RMBPT methods [8]. At wavelengths longer than 13.2 nm, non-lasing lines have been observed from laser produced plasmas (LPP). However, the twenty-one lines published in [9] left numerous $3d^94d$–$3d^94p$ and all $3d^94d$–$3d^94f$ transitions to be identified. Theoretical investigations of 4-4 transitions in [8] were limited to s-p and (partly) p-d transitions. In this work we report the identification of 53 transitions corresponding to Ni-like Cd ions based on spectra obtained from cadmium plasma columns generated using a fast capillary discharge. The spectroscopy of ions with such a high degree of ionization in discharge-created plasmas is made possible by a new type of fast capillary discharge that operates at peak currents of up to 200 kA and current risetimes exceeding 1.5×10^{13} A/s [10]. Relative to laser-created plasmas these capillary discharge plasmas have a lower electron density. Consequently, the spectra of these capillary discharge plasmas are clearly dominated by lines and often present a very small continuum background, which constitutes an advantage for the identification of spectral lines.

The next section discusses the plasma generation technique used as well as the spectroscopic tools used to acquire and calibrate the spectra. The theoretical computation used for interpretation of the spectra and for the line assignment is described in Section 3.

2. Plasma generation set-up and spectrometer calibration

The Cd plasmas were generated by exciting capillary channels filled with Cd vapor using a high power density pulse generator [11] that produces current pulses with a peak amplitude of up to 200 kA and a 10–90% rise time of 10–15 ns. Utilizing this discharge, Cd plasma columns were generated in polyacethal $(CH_2O)_n$ capillaries with diameters of 5 mm. The pulsed power generator consists of three pulse compression stages. The first two stages consist of a conventional Marx generator and 26 nF coaxial water-dielectric capacitor that has the purpose of rapidly charging the third and final pulse compression stage. The eight-stage Marx generator was operated at an erected voltage of ~650kV. The second compression stage is charged in about 1 μs. In turn this water capacitor is discharged through a self-breakdown spark gap pressurized with SF_6 gas to charge the third and final stage in about 75 ns. The third stage consists of two radial water dielectric transmission lines connected in a Blumlein configuration. The fast current pulse that excites the capillary plasma is produced by discharging the Blumlein transmission line through an array of seven synchronized triggered spark-gap switches distributed along the outer diameter of the water transmission line. This circular array of gas pressurized spark-gaps approximates a large single multi-channel spark gap, allowing for a very rapid switching of the Blumlein. The capillary load is placed in the axis of the Blumlein, which together with the spark gap array defines a very low inductance loop that allows for the generation of very fast current risetimes, exceeding 1.5×10^{13} A/s. The ground electrode is designed to have a central hole that allows for the observation of the axially emitted plasma radiation. The current pulse corresponding to each discharge shot was measured with a Rogowsky coil having a response risetime of less than 1 ns. Cd vapor was injected into the capillary through the hollow anode electrode of the capillary discharge. The Cd vapor was produced by a metal vapor gun designed to generate Cd vapor in a room temperature environment by rapidly

* Rocca@engr.colostate.edu
** Francois.Wyart@lac.u-psud.fr

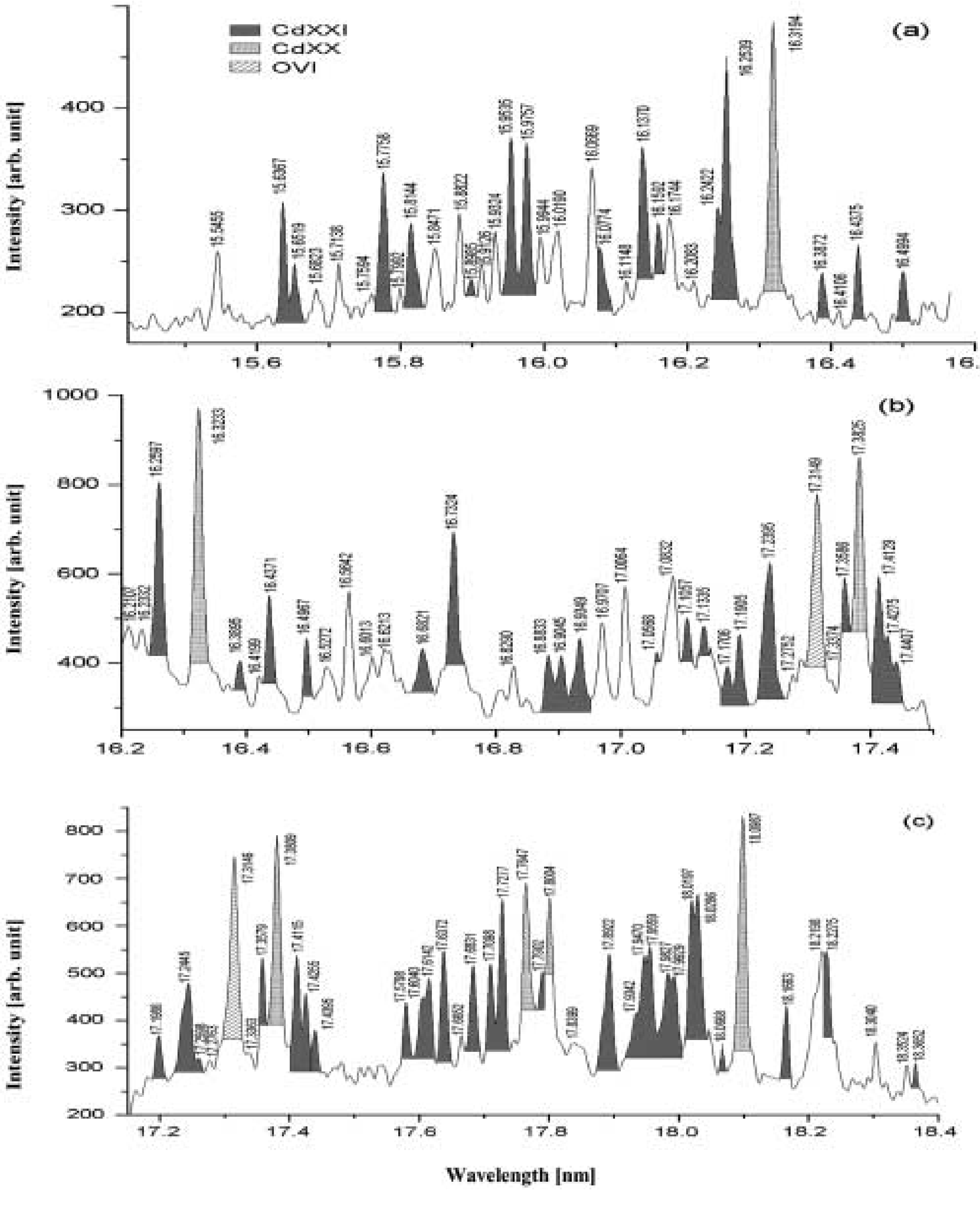

Fig. 1. (a–c) Spectra of a cadmium capillary discharge plasma column for the 15.4–18.4 nm wavelength region. Each spectrum corresponds to a single discharge pulse and was acquired with time resolution of 5 ns at 31.5, 34, and 40 ns after the initiation of the current pulse respectively. The current had peak amplitudes of 178, 188, and 182 kA respectively. The capillary diameter was 5 mm. Each spectral line is identified with the experimental wavelength resulting for the calibration corresponding to that particular shot. The difference in the wavelength of the lines appearing in the overlapping regions are illustrative of the error associated with the measurements. Some of the experimental wavelengths of the lines listed in table III are averages of two or more spectra.

heating a cadmium electrode with a capacitive discharge. Following its injection into the capillary channel, the Cd vapor was pre-ionized with a low current pulse preceding the fast high current pulse. Typically several tens of shots were made with each capillary. Observation of the plasma columns with a soft X-ray pinhole camera shows the current pulse rapidly compresses the plasma to form a hot and dense plasma at the capillary axis. A cylindrical shock

Table I. *Characteristics of the presently available theoretical studies by means of generalized least-squares (GLS) fits for $3d^9 4l$ configurations with the number of different ions* N_{ions}, *total number of levels* N_{lev} *and of adjustable parameters* N_{par}, *the average of deviations, and the gain in* N_{lev}/N_{par} *ratio in comparing individual and generalized least-squares.*

Config	N_{ions}	N_{lev}	N_{par}	$\langle \Delta E \rangle$ (cm^{-1})	$N_{\text{lev}}/N_{\text{par}}$ *ILS*	$N_{\text{lev}}/N_{\text{par}}$ GLS
$3d^94s$	19	75	26	10	1.3	2.9
$3d^94p$	23	233	41	46	1.5	5.7
$3d^94d$	21	228	38	95	2	6
$3d^94f$	19	171	31	140	2.2	5.5

wave shell is driven towards the axis of the discharge by the Lorentz force and by large thermal pressure gradients that arise near the capillary wall [11]. Pinhole camera measurements show the onset of significant soft X-ray emission occurs about 27 ns after the initiation of the current pulse, with rapidly increasing intensity in the few ns after that. The diameter of the soft X-ray emitting regions decreases as the plasma column compresses, until it achieves a minimum diameter of 250–350 μm at 32–34 ns after the onset of the current. Shortly afterwards the emitted soft X-ray intensity rapidly decreases.

The radiation axially emitted by the plasma was focused by a gold-coated grazing-incidence mirror into the slit of a 2.217 m grazing-incidence spectrograph. The spectrograph contained a 2400 lines per millimeter gold-coated diffraction grating mounted at an angle of incidence of 85.8 degrees. The detector consisted of a stack of two microchannelplates (MCP) in chevron configuration, a phosphor screen, and a CCD detector array. The CCD consisted of a front illuminated array of 1024 by 1024 pixels of 24 μm size that was thermoelectrically cooled. All the spectra have a temporal resolution of about 5 ns obtained by gating the MCPs with a voltage pulse. Time resolved spectroscopy was carried out through selected intervals in the spectral range between 10 and 20 nm. The spectral calibration was performed utilizing the wavelengths of known ionic transitions from capillary wall ablated material and from selected gases injected into the capillary channel. The spectral region between 12.7 nm and 13.6 nm was calibrated with lines of FVII, ArVIII, OVI and OVII [12]. The spectral region expanding from 15.4 nm to 18.4 nm was calibrated using numerous transitions of Ar ions corresponding to different stages of ionization ranging from ArX to ArXIV [12]. An indication of the error involved in the calibrations was obtained through a comparison with published wavelength of four CdXX lines [13–15]. All the presently observed CdXX lines were within 0.004 nm of the published values. From these results, from a similar comparison for OVI lines, and from the shot to shot variations of the measured wavelengths, the error in the measured transition wavelengths we are reporting can be conservatively estimated at 0.01 nm.

Table II. *Energy levels of CdXXI. Levels are designated in (J1, j2) coupling scheme, with* J *and* N *index numbering from the lowest level in its* J*-value for the configuration. The (J1, j2) purity in % is followed by SL leading components and purities. The experimental energies are from [9] for* $3d^94s$ *and* $3d^94p$ *and from the present work for* $3d^94d$ *and* $3d^94f$. E_{GLS} *are from the present work. Values are in cm*$^{-1}$.

Config.	Multiplet	J	Nth	%	SL %	E_{exp}	E_{GLS}
$3d^{10}$	^{1}S	0	1			0	0
$3d^94s$	(5/2,1/2)	3	1	100	^{3}D 100	3059268	3059362
	(5/2,1/2)	2	1	99	^{3}D 51	3066123	3066109
	(3/2,1/2)	1	1	100	^{3}D 100	3116960	3116938
	(3/2,1/2)	2	2	99	^{1}D 51	3122430	3122466
$3d^94p$	(5/2,1/2)	2	1	96	^{3}P 67	3389332	3389541
	(5/2,1/2)	3	1	99	^{3}F 50	3396397	3396372
	(3/2,1/2)	2	2	94	^{3}F 85	3448887	3448903
	(3/2,1/2)	1	1	74	^{3}P 58	3456137	3455958
	(5/2,3/2)	4	1	100	^{3}F 100	3467062	3467084
	(5/2,3/2)	2	3	91	^{1}D 62	3477956	3477946
	(5/2,3/2)	1	2	73	^{1}P 82	3482340	3482343
	(5/2,3/2)	3	2	99	^{3}D 74	3486540	3486478
	(3/2,3/2)	0	1	100	^{3}P 100	3511162	3511163
	(3/2,3/2)	3	3	100	^{3}F 49	3530843	3530922
	(3/2,3/2)	1	3	92	^{3}D 59	3533498	3533337
	(3/2,3/2)	2	4	99	^{3}D 57	3541520	3541628
$3d^94d$	(5/2,3/2)	1	1	71	^{3}S 78	3986980	3987347
	(5/2,3/2)	4	1	98	^{3}G 57	4011530	4011763
	(5/2,3/2)	2	1	89	^{3}P 48	4015240	4015035
	(5/2,3/2)	3	1	90	^{3}D 42	4023220	4022741
	(5/2,5/2)	1	2	72	^{1}P 51	4021200	4020881
	(5/2,5/2)	5	1	100	^{3}G 100	4021720	4021807
	(5/2,5/2)	3	2	89	^{3}D 44	4035150	4035181
	(5/2,5/2)	2	2	85	^{1}D 41	4040060	4040192
	(5/2,5/2)	4	2	98	^{3}F 79	4041400	4041522
	(5/2,5/2)	0	1	51	^{3}P 99	4047700	4047797
	(3/2,3/2)	1	3	71	^{1}P 48	4064580	4064639
	(3/2,3/2)	3	3	94	^{3}G 75	4068540	4068039
	(3/2,3/2)	2	3	99	^{3}F 64	4088350	4088228
	(3/2,3/2)	0	2	51	^{1}S 99	4241750	4241992
	(3/2,5/2)	1	4	71	^{3}D 52	4078130	4077736
	(3/2,5/2)	4	3	98	^{1}G 41	4085780	4086008
	(3/2,5/2)	2	4	97	^{3}D 43	4092000	4092296
	(3/2,5/2)	3	4	97	^{3}F 53	4098500	4098302
$3d^94f$	(5/2,5/2)	0	1	100	^{3}P 100		4566753
	(5/2,5/2)	1	1	79	^{3}P 89		4572294
	(5/2,5/2)	5	1	97	^{3}H 55	4587620	4587649
	(5/2,5/2)	2	1	74	^{3}P 63		4581343
	(5/2,5/2)	3	1	51	^{3}D 53	4597000	4597387
	(5/2,5/2)	4	1	64	^{3}F 75	4603200	4601625
	(5/2,7/2)	2	2	70	^{1}D 40		4596250
	(5/2,7/2)	6	1	100	^{3}H 100	4585810	4585548
	(5/2,7/2)	4	2	62	^{1}G 48	4603880	4603935
	(5/2,7/2)	5	2	96	^{3}G 76	4606060	4606237
	(5/2,7/2)	3	2	50	^{1}F 49	4608720	4608621
	(5/2,7/2)	1	2	51	^{3}D 85		4617234
	(3/2,7/2)	2	3	86	^{3}D 36		4641317
	(3/2,7/2)	4	3	93	^{3}H 73	4648520	4647106
	(3/2,7/2)	5	3	98	^{1}H 39	4651300	4651369
	(3/2,7/2)	3	4	99	^{3}G 63	4667900	4667627
	(3/2,5/2)	2	4	90	^{3}F 63		4655651
	(3/2,5/2)	3	3	98	^{3}F 41	4660660	4660602
	(3/2,5/2)	4	4	96	^{3}G 46	4666370	4666127
	(3/2,5/2)	1	3	67	^{1}P 93		4725764

3. Interpretation of the energy levels of CdXXI

The first excited configurations $3d^9nl$ of Ni-like ions have been studied by means of the chain of programs of L.A.C. [16] in the Slater–Racah approach, as described by Cowan [17]. In this perturbative method, a number N_P of radial

Table III. *Classification of lines of Nickel-like CdXXI. The first column shows the calculated wavelengths (λ_{cal} in nm) as they are derived from the "best" experimental level values in Table II, the second and third columns show the experimental wavelengths (λ_{exp}) and wavenumber. Int is the measured relative intensity. The level designations imply the* J-*value and index* N_{th}*, which numbers the levels from the lowest energy in the same* J-*values and configuration, as used in [9]. The emission transition probability* gA *(in $10^{10}\ s^{-1}$) in length form is derived by means of Cowan codes for* E_{GLS} *level values with no C.I. effects included.*

λ_{cal} (nm)	λ_{exp} (nm)	σ (cm^{-1})	Int	$\lambda_{exp} - \lambda_{cal}$ (nm)	Jo *N*th		Je *N*th	E_{odd}		E_{even}	*gA*	Comment
12.7289	12.7349	785244		0.0060	4p 1 1		4d 0 2	3456137		4241750	21	
13.1681	13.1618	759774	4	−0.0063	4p 1 2	–	4d 0 2	3482340	–	4241750	164	
15.6381	15.6367	639521	4	−0.0014	4p 2 2	–	4d 2 3	3448887	–	4088350	219	
15.6555	15.6519	638900	2	−0.0036	4p 3 1	–	4d 3 2	3396397	–	4035150	39	
15.7757	15.7758	633882	5	0.0001	4p 2 1	–	4d 3 1	3389332	–	4023220	266	
15.8175	15.8144	632335	3w	−0.0031	4p 1 1	–	4d 2 3	3456137	–	4088350	134	
15.8921	15.8985	628990	1	0.0064	4p 2 2	–	4d 1 4	3448887	–	4078130	14	
15.9535	15.9535	626822	6	0.0000	4p 3 1	–	4d 3 1	3396397	–	4023220	329	
15.9768	15.9757	625951	6	−0.0011	4p 2 1	–	4d 2 1	3389332	–	4015240	381	
16.0774	16.0774	621991	2b	0.0000	4p 1 1	–	4d 1 4	3456137	–	4078130	32	
16.1381	16.1370	619694	6	−0.0011	4p 2 2	–	4d 3 3	3448887	–	4068540	570	
16.1592	16.1592	618842	3	0.0000	4p 3 1	–	4d 2 1	3396397	–	4015240	81	
16.2419	16.2422	615680	2b	0.0003	4p 2 2	–	4d 1 3	3448887	–	4064580	22	
16.2566	16.2568	615127	8	0.0002	4p 3 1	–	4d 4 1	3396397	–	4011530	858	
	16.3214	612693	9									CdXX
16.3829	16.3884	610188	1	0.0055	4p 2 3	–	4d 2 3	3477956	–	4088350	24	
16.4354	16.4373	608372	3	0.0019	4p 1 1	–	4d 1 3	3456137	–	4064580	144	
16.5014	16.4981	606130	2	−0.0033	4p 1 2	–	4d 2 3	3482340	–	4088350	90	
16.6845	16.6821	599444	1	−0.0024	4f 3 4	–	4d 3 3	4667900	–	4068540	106	
16.7323	16.7324	597643	7	0.0001	4p 2 1	–	4d 1 1	3389332	–	3986980	229	
16.8819	16.8833	592301	2	0.0014	4f 4 2	–	4d 4 1	4603880	–	4011530	127	
16.9044	16.9045	591558	3	0.0001	4p 1 1		4d 0 1	3456137	–	4047700	89	
16.9324	16.9349	590497	3	0.0025	4p 2 3	–	4d 3 3	3477956	–	4068540	92	
17.0572	17.0568	586276	3	−0.0004	4p 2 2	–	4d 3 2	3448887	–	4035150	72	
17.1031	17.1057	584600	3	0.0026	4f 5 2	–	4d 5 1	4606060	–	4021720	173	
17.1255	17.1335	583652	3w	0.0080	4p 1 1	–	4d 2 2	3456137	–	4040060	56	
17.1750	17.1706	582391	2	−0.0044	4p 1 2	–	4d 1 3	3482340	–	4064580	37	
17.1892	17.1946	581578	4	0.0054	4f 3 1	–	4d 2 1	4597000	–	4015240	250	
17.2420	17.2420	579979	4w	0.0000	4f 4 1	–	4d 3 1	4603200	–	4023220	394	Tentative, Blend
17.2420				0.0000	4f 4 3	–	4d 3 3	4648520	–	4068540	797	Tentative, Blend
17.2548	17.2598	579381	2	0.0050	4f 3 4	–	4d 2 3	4667900	–	4088350	485	
17.3584	17.3583	576093	6	−0.0001	4f 5 1	–	4d 4 1	4587620	–	4011530	964	
	17.3817	575318	10									CdXX
17.4114	17.4122	574310	5	0.0008	4p 4 1	–	4d 4 2	3467062	–	4041400	234	
17.4283	17.4265	573839	3	−0.0018	4f 3 1	–	4d 3 1	4597000	–	4023220	225	
17.4347	17.4401	573391	2	0.0054	4f 3 2	–	4d 3 2	4608720	–	4035150	118	
17.5852	17.5798	568835	3	−0.0054	4f 3 3	–	4d 2 4	4660660	–	4092000	502	Blend
17.5852				−0.0054	4f 3 2	–	4d 2 2	4608720	–	4040060	384	Blend
17.5830				−0.0032	4f 4 2	–	4d 3 2	4603880	–	4035150	521	Blend
17.6097	17.6040	568053	4	−0.0057	4f 4 4	–	4d 3 4	4666370	–	4098500	683	
17.6163	17.6142	567724	4	−0.0021	4p 3 3	–	4d 3 4	3530843	–	4098500	151	
17.6377	17.6372	566983	5	−0.0005	4p 0 1	–	4d 1 4	3511162	–	4078130	135	
17.6828	17.6831	565512	4	0.0003	4f 5 3	–	4d 4 3	4651300	–	4085780	951	Blend
17.6878				−0.0047	4p 1 2	–	4d 0 1	3482340	–	4047700	10	Blend
17.7098	17.7098	564659	4	0.0000	4f 5 2	–	4d 4 2	4606060	–	4041400	794	
17.7276	17.7277	564089	6	0.0001	4f 6 1	–	4d 5 1	4585810	–	4021720	1118	
	17.7647	562914	7									CdXX
17.7885	17.7902	562107	3p	0.0017	4f 3 3	–	4d 3 4	4660660	–	4098500	89	Blend
17.7903				−0.0001	4p 2 3	–	4d 2 2	3477956		4040060	220	Blend
	17.8004	561785	6									CdXX
17.9050	17.8922	558903	4w	−0.0128	4p 1 3	–	4d 2 4	3533498	–	4092000	248	
17.9301	17.9342	557594	2s	0.0041	4p 1 2	–	4d 2 2	3482340	–	4040060	94	Blend
17.9370				−0.0028	4p 3 3	–	4d 2 3	3530843	–	4088350	18	Blend
17.9471	17.9470	557196	4	−0.0001	4p 2 3	–	4d 3 2	3477956	–	4035150	292	
17.9540	17.9559	556920	5	0.0019	4p 2 4	–	4d 3 4	3541520	–	4098500	434	
17.9805	17.9827	556090	3	0.0022	4p 4 1	–	4d 3 1	3467062	–	4023220	41	CdXIX
17.9986	17.9929	555775	3s	−0.0057	4f 3 1	–	4d 4 2	4597000	–	4041400	30	
18.0226	18.0197	554948	7	−0.0029	4p 3 2	–	4d 4 2	3486540	–	4041400	530	Blend
18.0201				−0.0004	4p 3 3	–	4d 4 3	3530843	–	4085780	735	Blend
18.0291	18.0286	554674	7	−0.0005	4p 4 1	–	4d 5 1	3467062	–	4021720	897	
18.0662	18.0668	553501	1	0.0006	4p 3 2	–	4d 2 2	3486540	–	4040060	18	
	18.0987	552525	10									CdXX
18.1660	18.1663	550470	3	0.0003	4p 2 4	–	4d 2 4	3541520	–	4092000	146	
18.2279	18.2275	548621	4p	−0.0004	4p 3 2	–	4d 3 2	3486540	–	4035150	185	
18.3666	18.3652	544508	1	−0.0014	4p 4 1	–	4d 4 1	3467062	–	4011530	61	

integrals R^k and ζ_{nl} bound with electrostatic and spin–orbit interactions are processed as adjustable parameters P determined by least-squares fit from N_{lev} known experimental energy levels ($N_{\text{lev}} > N_{\text{par}}$) of an electronic configuration in the studied ion. Initially separate studies of the spectra from ZnIII till BrVIII had led to accurate values of angular coefficients $\partial E/\partial P$ in intermediate coupling. This made possible a comprehensive survey of $3d^9 4s$, -4p and -4d by means of generalized least squares (GLS) from levels of all ions simultaneously, aiming to increase the ratio $N_{\text{lev}}/N_{\text{par}}$. For that purpose, the electrostatic Slater parameters were replaced by $R^k = A(R^k) + B(R^k) \cdot Z_c + C(R^k)/(Z_c + D)$ according to Edlén [18] (Z_c = charge of the ionic core) and the spin–orbit parameters were expressed as polynomials $\zeta_{nl} = c_0 + c_1 \cdot Z_c + \cdots + c_4 \cdot Z_c{}^4$. The GLS constants $A(R^k)$, $B(R^k)$, $C(R^k)$ and c_i fitted from the sequence ZnIII–BrVIII were used to predict levels of ions till MoXV [19] and, after their discovery [20], till SnXXIII [21]. This guided the search for new levels beyond MoXV and the classification of 17 lines as 4s-4p transitions and 2 lines as 4p-4d transitions in laser produced plasma spectra of cadmium [9] were derived from these GLS studies. After 1988, the 4p-4d transitions of potential interest for soft X-ray lasers were surveyed [22], initial identifications of some $4d\,^1S$–$4p\,^1P$ transitions were revised recently [2] and the KrIX spectrum was observed and interpreted at Troitsk [23].

Systematic discrepancies $\lambda_{\text{exp}} - \lambda_{\text{GLS}}$ had been noticed beyond MoXV in the wavelengths of 4p-4d transitions [21] and, in the present step, the reliability of the GLS levels was increased by using more stringent conditions and extended sets of experimental levels. The present study differs from earlier ones in two points:

1. The radial parameters were replaced by their scaling factors $SF(P) = P/P_{\text{HFR}}$, by multiplying the angular coefficients $\partial E/\partial P$ by P_{HFR} values obtained from the RCN codes of Cowan [17]. It is a known fact that scaling factors are very consistent in neighboring elements and close to 1. First isoelectronic GLS studies in multicharged copper-like ions used successfully SF's as adjustable parameters [24].
2. The experimental error on the energies in the fit ranges from $0.3\,\text{cm}^{-1}$ in ZnIII to $\sim 200\,\text{cm}^{-1}$ for $Z_c > 25$. Therefore the levels were weighted as $Z_c{}^{-1}$.

The main features of the four GLS studies are collected in Table I. For $3d^9 4f$, which uses some recent data on 4d-4f transitions [25], no GLS study had been performed.

The average of deviations $\Delta E = E_{\text{exp}} - E_{\text{GLS}}$ in column 5 increases from $3d^9 4s$ to $3d^9 4f$, partly due to mixing with other configurations which are not considered in our "single" configuration model. $3d^9 4s$ and $3d^9 4p$ are isolated in all ions studied here, whereas $3d^9 4d$ is overlapped by $3d^9 5s$ and $3d^8 4s^2$ at $Z_c = 3, 4$ and $3d^9 4f$ by $3d^8 4s4p$ and $3d^9 np$ in several low-Z_c ions (see BrVIII [26]). In the latter configurations, the most perturbed levels were discarded in the fitting process. Two levels of $3d^9 4f$ with $J = 4$ are derived from a line at 17.242 nm. In the present step of GLS calculations, it was not possible to reduce the large deviations $E_{\text{exp}} - E_{\text{GLS}}$ with a reasonable set of fitted parameters and the classified line and levels are reported as tentative.

The predicted levels of CdXXI are collected in Table II and are compared with energies derived from the classified lines of Table III. For $3d^9 4s$ and $3d^9 4p$, the energies are those of [9]. Two couplings are given and the $J_1 - j_2$ coupling leads generally to more realistic designations than does Russell–Saunders. In the recent publication [8] using the RMBPT method, the transition energies of Ni-like ions from Ag to Sn were reported for 3–4 resonance transitions, and for 4s-4p and 4p-4d transitions, except both $3d^9 4d$ $J = 0$ levels. For CdXXI, the published 4-4 transitions are close to λ_{exp} and λ_{GLS} values. For the 53 lines reported in Table III, the average deviation $\langle \lambda_{\text{exp}} - \lambda_{\text{th}} \rangle$ is 0.0080 nm for the relativistic MBPT method and 0.0065 nm for the present GLS study. In terms of energies E_{MBPT} relative to the ground state, systematic deviations appear.

Several cadmium lines are still uninterpreted and they might belong to other ions. Comparisons with the zinc-like lines reported in [9] were not conclusive. It is noticed that the strongest of those lines are close to 4-4 transitions of CdXXII as we derive them from scaled Cowan-type calculations. As the CoI isoelectronic sequence is too poorly known, this did not lead so far to definite conclusions.

4. Conclusions

Fifty-three transitions corresponding to Ni-like Cd ions have been identified from the spectra of high current capillary discharge plasma columns. The average deviation between the measured and theoretical wavelength values is $\langle \lambda_{\text{exp}} - \lambda_{\text{th}} \rangle = 0.0065$ nm for the GLS method used in the present study, as compared to 0.0080 nm for the MBPT method. The results demonstrate that fast capillary discharges can produce clean spectra for the study of multiply charged ions with charges of up to at least $Z = 20$. The newly identified Ni-like Cd lines can be used in combination with other Cd ion transitions reported in the literature in the plasma diagnostics necessary for the development of efficient Ni-like Cd lasers operating at a wavelength of 13.2 nm.

Acknowledgement

This work was supported by DARPA grant G_DAAD 19-99-1-0279 and by the National Science Foundation. The Colorado State University researchers also gratefully acknowledge the support from the W. M. Keck Foundation. The Laboratoire Aime Cotton is associated with Universite Paris-Sud. We acknowledge the contributions of Maximo Frati and Fernando Tomasel to the generation of the Cd capillary plasmas and thank V. N. Shlyaptsev for useful discussions.

References

1. Zhang, J. *et al.*, Phys. Rev. Lett. **78**, 3856 (1997).
2. Li, Y. *et al.*, Phys. Rev. A **58**, R2668 (1998).
3. Daido, H., Ninomiya, S., Takagi, M., Kato, Y. and Koike, F., J. Opt. Soc. Am B **16**, 296 (1999).
4. Dunn, J. *et al.*, Phys. Rev. Lett. **84**, 4834 (2000).
5. Spector, N. *et. al.*, J. Phys. B: At. Mol. Opt. Phys. **17**, L275 (1984).
6. Quinet, P. and Biémont, É., Physica Scripta **43**, 150 (1991).
7. Renaudin, P. *et al.*, in "UV and X-Ray Spectroscopy of Laboratory and Astrophysical Plasmas," (Eds. E. Silver and S. Kahn) (Cambridge University Press, 1993) p. 157.
8. Safronova, U. I., Johnson, W. R. and Albritton, J. R., Phys Rev. A **62**, 052505 (2000).

9. Churilov, S. S., Ryabtsev, A. N. and Wyart, J.-F., Physica Scripta **38**, 326 (1988).
10. Gonzalez, J. J., Frati, M., Rocca, J. J., Shlyaptsev, V. N. and Osterheld, A. L., Phys. Rev. E **65**, 026404 (2002).
11. Sakadzik, S. *et al*., Soc. Photo-Opt. Instrum. Eng. J. **4505**, 35 (2001).
12. Kelly, R. L., J. Phys. Chem. Ref. Data. **16**, 1 (1985), R. L. Kelly and L. J. Palumbo, "Atomic and Ionic Emission Lines Below 2000 Angstroms," NRL Report 7599 (1973).
13. Reader, J., Acquista, N. and Cooper, D., J. Opt. Soc. Am. B **73**, 1765 (1983).
14. Ivanov, L. N., Ivanova, E. P., Kononov, E. Ya., Churilov, S. S. and Tsirekidze, M. A., Physica Scripta **33**, 401 (1986).
15. Seely, J. F., Brown, C. M. and Feldman, U., At. Data Nucl. Data Tab. **43**, 145 (1989).
16. Bordarier, Y., Bachelier, A. and Sinzelle, J., Chain of Programs AGENAC, ASSAC, DIAGAC, GRAMAC, Laboratoire Aimé Cotton, Orsay (1980).
17. Cowan, R. D., "The Theory of Atomic Structure and Spectra," (University of California Press, Berkeley, 1981) and computer codes.
18. Edlén, B., in "Encyclopedia of Physics," Vol. XXVII, Springer Verlag, Berlin (1964).
19. Wyart, J.-F. and Ryabtsev, A. N., Physica Scripta **33**, 215 (1986).
20. Ryabtsev, A. N., Churilov, S. S. and Wyart, J.-F., Opt. I. Spektr. **62**, 258 (1987).
21. Wyart, J.-F., Physica Scripta **36**, 234 (1987).
22. Scofield, J. H. and MacGowan, B. J., Physica Scripta **46**, 361 (1992).
23. Ryabtsev, A. N., Antsiferov, P. S., Nazarenko, V. I., Churilov, S. S. and Wyart, J.-F., J. Physique IV, **11**, 317, (2000).
24. Wyart, J.-F., Ryabtsev, A. N. and Reader, J., J. Opt. Soc. Am. **71**, 692 (1981).
25. Ryabtsev, A. N. *et al*., Opt. I. Spektr. **87**, 197 (1999).
26. Churilov, S. S. and Joshi, Y. N., Physica Scripta **53**, 431 (1996).